Is Earth's Surface Insolation Increasing? – Implication for Climate Change Theories

José L. Fernández-Solís [*] and Bo Young Kim[**]

Foreword

This article was released in 2023 and based on 25 years of consecutive data gathering, as explained. The authors planned to update the content after 5 years. However, the advent of an earlier and more intense solar cycle 25 maxima in 2023 coupled with research indicating further and faster weakening of Earth Magnetic Field, and an extraordinary large and earlier ozone hole has led us to investigate what the last two years of data gathering are doing to our collective total. What we have found and are reporting is a substantial increase in the amount of insolation that Earth is receiving. Staggering numbers that have not found the daylight of the public press.

Abstract

This paper investigates four critical questions:

First, has the amount of solar irradiance that the Earth receives (Global horizontal irradiance) increased over time? This question requires that scientific instruments have recorded, over time, data about solar irradiance. Fortunately, such instruments do exist, and the data has been kept and is available for researchers. The United States' National Oceanic and Atmospheric Administration's (NOAA) Surface Radiation budget (SURFRAD) network has seven stations recording the same type of data over time. The data is available and can be analyzed across different spectrums, (NOAA, 2005). Therefore, Earth-ground insolation data from SURFRAD network was analyzed to answer the question. As a result, it was shown that the solar irradiance of the Earth's surface had an increasing trend over the years observed at five out of seven stations in the network, and that the amount increased was significant.

Second, what does the upward trend in this data reveal? An upward trend, as found in most stations, indicates a slight increase of solar irradiance at surface level by more than one percent during twenty-five years of observation.

Third, is this trend significant? The Earth facing the sun always receives 410×10^{18} Joules each hour! A one-percent increase means 410×10^{16} Joules per hour! In comparison, the total amount of energy that humans **use in a year** is 410×10^{18} Joules, (Harrington, 2015).

Current theories indicate that global warming due to anthropogenic forcing causes solar radiation to bounce from the different layers of the Earth's atmosphere. If this theory is correct, Earth should be receiving less and not more solar irradiance at ground level, (Brown, Maxwell et al. 2018).

Fourth, what mechanism could allow more solar rays to penetrate all atmospheric layers, plus, increase irradiance? One theory is that the Earth's magnetic shield is weakening allowing the kind of irradiance to reach Earth's surface at increasing levels, as found in this research analysis, (Brooks 2019, and Budyko 1969).

The implications from the data are clear, nothing heats the planet like the sun. There is no anthropogenic mechanism that has the capacity nor the potential, to increase Earth's warming like additional sun rays penetrating Earth's magnetic shield due to its weakening. The cause of the Earth's shield weakening is treated in (Fernández-Solís 2018) research paper that raised the question: "Is there another strand of evidence on the scientific finding that Earth's magnetic field (the B-field) is weakening?"

* José L. Fernández-Solís, PhD – Emeritus Associate Instructional Professor, Texas A&M University jsolis@tamu.edu
** Bo Young Kim, PhD – Postdoctoral Fellow, NYU Grossman School of Medicine, by0705@gmail.com

This paper demonstrates that the solar energy Earth receives from the Sun has been increasing over the years through numerical evidence using the following format:

- Section 1 Introduction
- Section 2 Data and Preprocessing Methods
- Section 3 Adopted Analytical Method and Metrics
- Section 4 Results, Interpretations and Summary of Data
- Section 5 Comments and Conclusion

1. Introduction

Scientists have found that Earth's B-field is weakening. The weakening reason is attributed to an aperiodic Earth core flip that causes a magnetic pole flip. In other words, where the North Pole is now becomes the South Pole and vice versa. This pole flip has major consequences and implications critical to a normal Earth environment, (Brooks, 2019).

Earth core flip, like the Sun's more periodic flip every 11 years, is a chaotic event where the B-field lines become discontinuous and intertwines, it loses density, and becomes chaotic as NASA has proven and shown in (Fernández-Solís, 2018). In time the flip stops through a mechanism that is not known, the B-field lines resume continuity and gains strength, and chaos disappears in a new norma. This is the case of a complete flip. There is also the case of a core excursion when the core meanders and wobbles but does not flip in which case chaos reigns for a longer period of time.

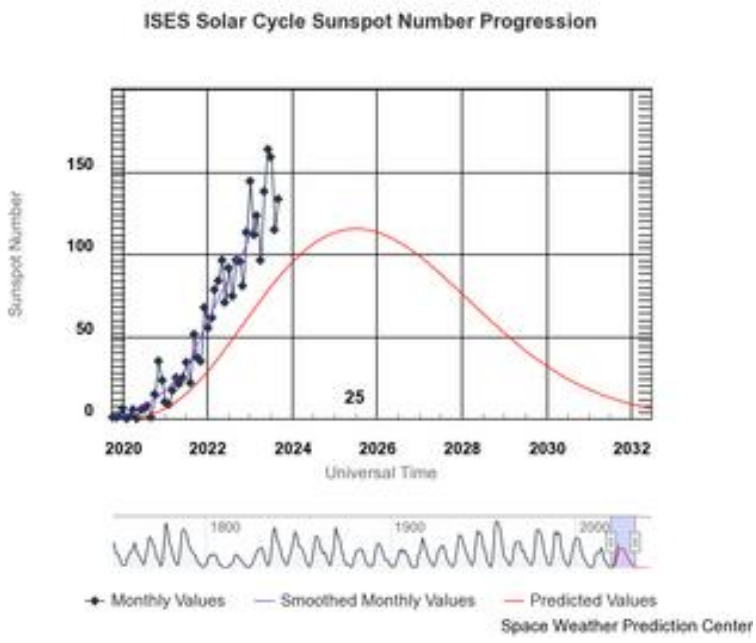

When the B-field loses strength, Earth's protection from solar radiation is weakened to the point that it is almost gone. The Sun provides an example of what happens during a magnetic flip (Široký, and Richard 2017. The Sun was at a solar minimum 2018-2022, where its magnetic field is continuous with hardly any solar flares. We are now on the Sun's 25th cycle since recording began, that is 25 cycles of 11 years approximately. It started in earnest in 2022 and has earlier and remarkable increased intensity, Figure 1.

Figure 1. Sun Cycle 25 (Credit: NASA/Goddard: space weather prediction center)

SWPC (Space Weather Prediction Center (https://www.swpc.noaa.gov/) reports that during this cycle 25, periodic incidents of dangerous solar radiation reaching the space station and affecting satellites in orbit. When an increase of solar radiation is detected whether at a solar maximum or minimum, satellite owners and the space station are warned. However, at a solar minimum with very few sunspots, the explanation for solar ray warnings could be that Earth's magnetic field has weakened and is no longer shielding these instruments from solar radiation as before, (Livermore et al. 2020).

Additional strands of evidence that the B-field is weakening are needed. (Vervelidou et al. 2017). Therefore, (Fernández-Solís, 2018) hypothesized that B-field weakening should allow additional Sun insolation to reach Earth's surface when measured over time, the premise of this paper.

The current research found that Earth-ground insolation has been continuously monitored over several decades and at multiple sites-readings that are available to the public, (Smulsky 2020). The data was found, collected, and analyzed to determine if there is a scientific trend on Earth-ground insolation, (Fedorov, and Grebennikov 2017).

Premise

Earth core flip leads to B-field flip causing B-field weakening allowing Earth-ground insolation to increase and thus contributing to climate change.

According to the US Department of Energy, nothing has the magnitude to affect Earth's climate like the energy coming from the Sun. If the research finds that over time there is an increase in Earth's ground insolation (probably due to B-field weakening), then Earth's climate change rhetoric will need to incorporate a much more significant source of global warming than carbon and other gases, (Harrington, 2015).

2. Data and Processing Methods

The NOAA Surface Radiation budget (SURFRAD) network was established in the mid-nineteen nineties to support climate research with reliable, continuous, long-term measurements of the surface radiation on a national scale (Augustine, et al. 2000; Augustine, et al. 2005; Yang, 2018).

2.1. SURFRAD Dataset

There are a total of seven observatory stations sparsely located in the U.S. : These locations were chosen to represent the diverse and varying climates of the U.S. Observations began in 1995 at the first four stations. The total observations extended to seven gradually by 2003. Daily data continues to be added and can be downloaded on SURFRAD's FTP server.

SURFRAD dataset includes ground-based irradiances and other meteorological data including air temperature and relative humidity. Data is reported as a 1-minute average (or 3-minute average by 1998). Quality of data is being monitored, and QC (quality control) flags are included in all raw data. Furthermore, calibrations are conducted and reported on SURFRAD's website constantly. The spectral range that SURFRAD's instruments measure includes ultraviolet (A, B and C), visible and infrared rays (NOAA 2005). The global horizontal irradiance is calculated using 'direct_n' and 'diffuse' if available, or 'dw_solar' if not. The following are names of instruments and the spectral ranges corresponding to each variable used by SURFRAD
from https://gml.noaa.gov/aftp/data/radiation/surfdrad/Bondville_IL/README:

- 'direct_n': The Normal Incidence Pyrheliometer (NIP).
  The NIP measures direct-normal solar radiation in the broadband spectral range from 280 to 3000 nm. In 2016, it was replaced by the Kipp and Zonen CHP1 pyrheliometer and it covers the total solar spectrum of solar radiation between 200 to 4000 nm (Augustine and Hodge, 2021).

- 'diffuse': Eppley 8-48 "black and white" pyranometer. (This has been used since 2001.)
  This instrument is sensitive to the broadband spectral range from 280 to 3000 nm.

- 'dw_solar': The Spectrolab SR-75 pyranometer.
  This instrument is sensitive to the broadband spectral range from 280 to 3000 nm.

The SURFRAD spectrum is the remnant of the solar wind filtered through the different layers of Earth's atmosphere as shown in Figure 2. Under highly weakened conditions ultraviolet (F1) and Xray (D) electrons are likely to reach Earth's surface.

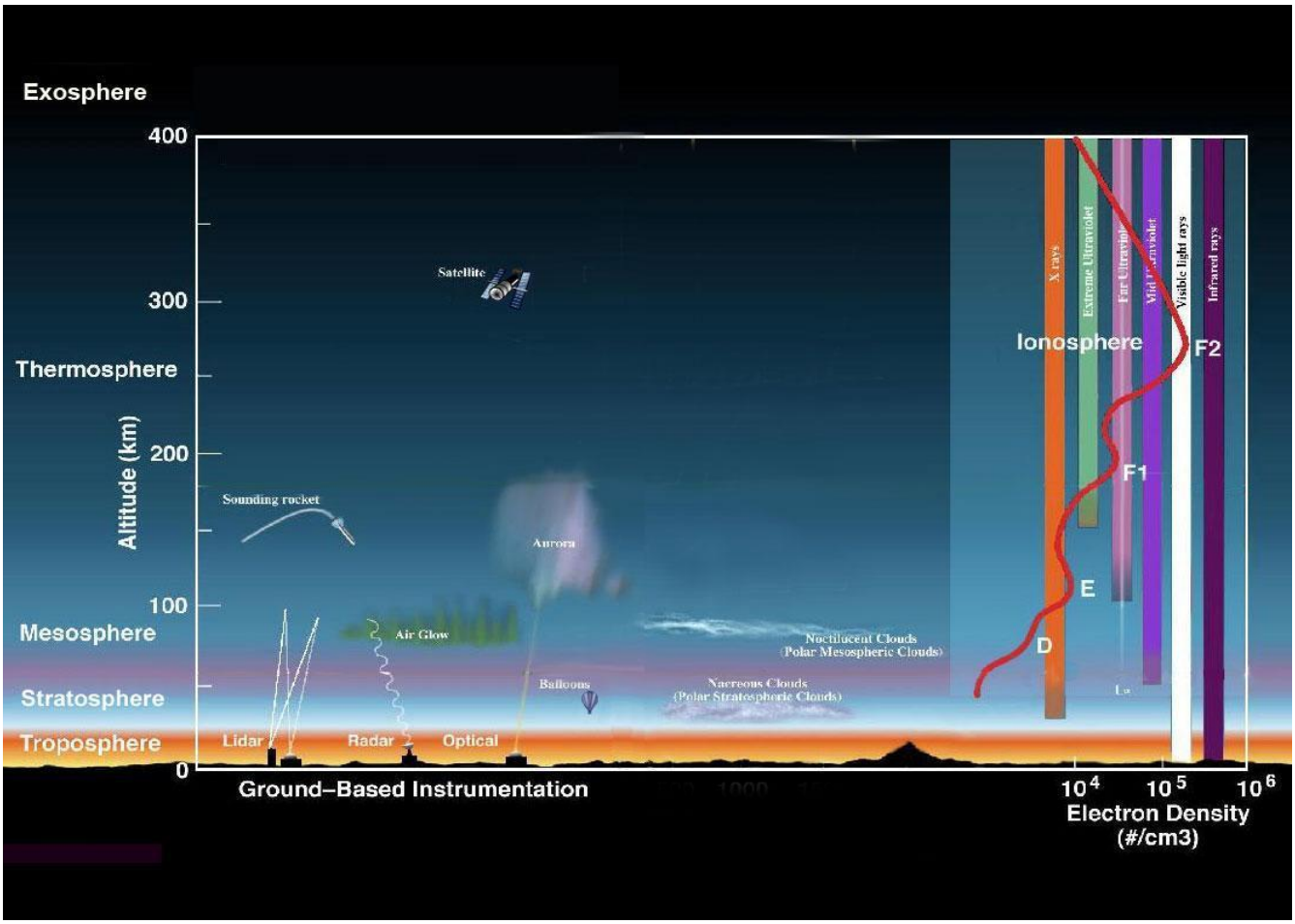

Figure 2. Atmospheric layers and electron densities under Earth magnetic shield's normal strength
(Credit: NASA/Goddard: https://www.nasa.gov/mission_pages/sunearth/science/atmosphere-layers2.html)

Figure 3 is a visual interpretation of the approximate wave range that SURFRAD instruments measure.

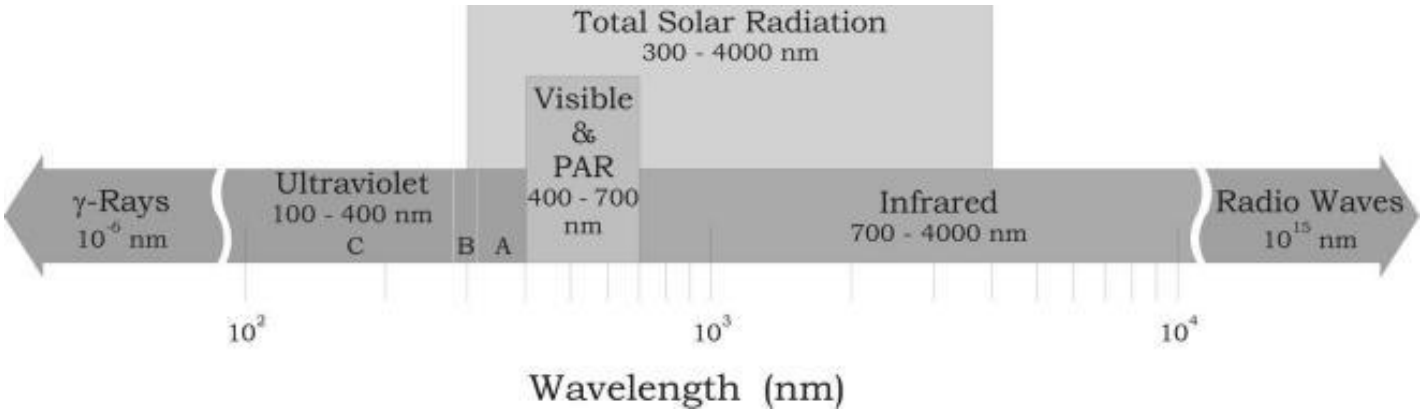

Figure 3. Total Solar radiation wavelengths

2.2. The Sun's Solar Wind, Coronal Mass Ejections and Earth Atmospheric Layers

The Sun is the origin of visible and invisible light. Invisible light is in the form of a continual outflow of plasma, ionized gas, waves and particles, the solar wind. Earth's atmosphere is protected from direct exposure to the solar wind by its magnetic field which forms a dynamic structure, the Van Allen Belt (discovered in 1958) at the magnetosphere around which the solar wind is diverted. The solar wind plasma carries electrical currents accelerated out of the sun's outer atmosphere at supersonic speeds. Besides the solar wind, the sun also expels intense releases of electromagnetic radiation during cyclic (we are in the 25th observation cycle) solar magnetic flips in what is called Coronal Mass Ejections (CME). CME's are transient, violent events when plasma plus radiation is expelled at speeds more than 1,000 Kilometers per second, and sometimes approaching the speed of light. On top of these two, there is the interplanetary magnetic field (IMF) that changes in density, speed, temperature, strength, and orientation, see Figure 4.

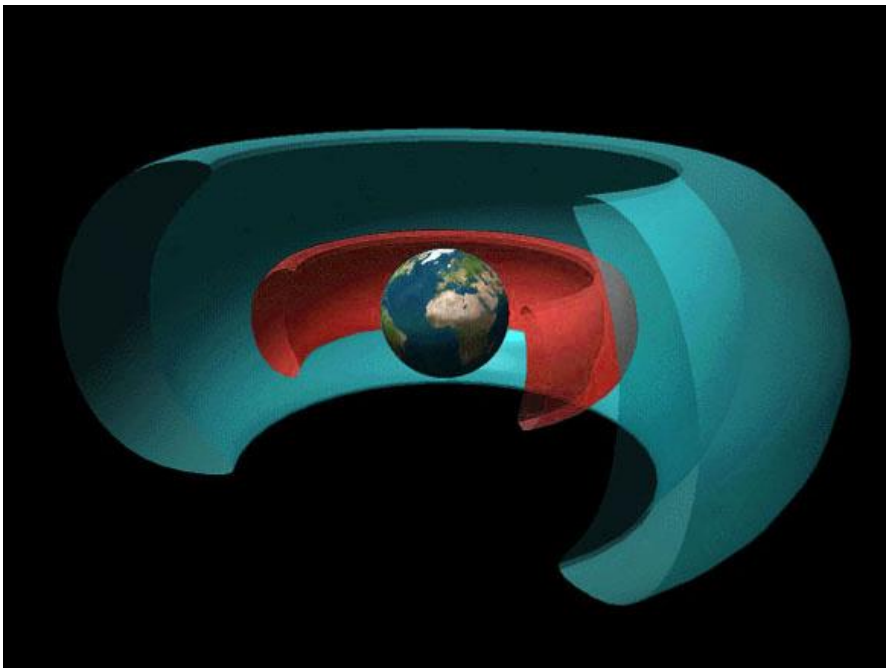

Figure 4. VanAllen radiation belts (Credit JHUAPL, NASA, recolored by cmglee - http://www.nasa.gov/content/goddard/van-allen-probes-reveal-zebra-stripes-in-spacehttps://earthobservatory.nasa.gov/images/78985/probing-the-electric-space-around-earth)

The solar wind, the CME and IMF encounter first the Earth's atmosphere at the Magnetosphere where the Van Allen Belts buffer some of the electro magnetized plasma and some radiation rays. Further down towards the Earth, at an altitude of approximately 80 Kilometers, the solar wind hits a population of mix glasses (ozone is one) of the thermosphere crating the ionosphere.

2.3 Atmospheric Ozone

New insights into the activity of solar wind high energy electrons have come from a simulation study led by geophysicist Yuto Katoh (2023). The ionosphere is a wide region between roughly 60 to 600 kilometers above Earth and includes the Mesosphere, Thermosphere, and Exosphere. Incoming electrons collide with gas molecules, a process that is heavily influenced by the effects of the geomagnetic field on the charged particles involved. The Tohoku team focused on simulating the effects of a relatively unstudied "mirror force" on electron precipitation. This mirror force is caused by the magnetic force acting on charged particles under the influence of the geomagnetic field, Figure 5.

The simulations demonstrated how the mirror force causes relativistic electrons to bounce back upwards, to an extent dependent on the angles at which the electrons arrive. The predicted effect means that the electrons collided with other charged particles higher in the ionosphere than previously suspected. This confirms the higher temperatures on the upper ionosphere where sun flux interacts with the geomagnetic field.

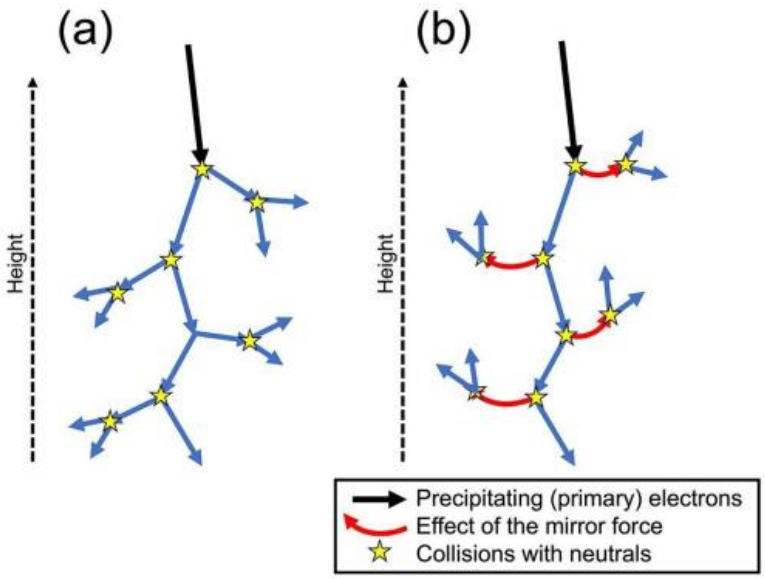

Illustration showing the relation between precipitating electrons, mirror force, and collisions with neutrals. The cases (a) without and (b) with mirror force are shown, indicating that the mirror force tends to move electrons upward through the collisions with neutrals. Credit: Yuto Katoh et al

Figure 5. Relation between precipitating electrons, mirror force, and collisions with neutrals

On the other hand, a weak or ineffective magnetic field allows the same particles to continue traveling downward towards Earth surface and warm it. Katoh explains that "Precipitating electrons that manage to pass through the mirror force can reach the middle and lower atmosphere, contributing to chemical reactions related to variations in ozone levels. Decreased ozone levels reduce protection ozone offers living organisms from additional ultraviolet radiation.

Ionizing radiation has so much energy it can knock electrons out of atoms, a process called ionization and the atoms then undergo radioactive decay. Examples of ionizing radiation are Alpha Particle (α), Beta Particles (β), Gamma Rays (γ), and X Rays (χ). χ rays are similar to Gamma rays in that they are photons of pure energy but come from different parts of the atom (χ rays from processes outside the nucleus and γ rays from inside the nucleus).

Several articles, (Reddmann et al 2023), go into great detail about Ionizing Radiation, such as Bodner Research Web and EPA Radiation Basics that has excellent graphics based on classical understanding of solar radiation. However, very recent scientific insights have shed new light on how the Geomagnetic field protects Earth from electron showers.

2.4. Area and Period of Interest

The SURFRAD network (Augustine, et al. 2000; Augustine, et al. 2005) is shown in Figure 6. The stations are divided into two groups: Station group 1 and Station group 2. The results are explained separately. Stations in group 2 have a shorter time observation period than the ones in group 1.

A small difference in the observation period could affect the results given that the observation periods are not long at all stations; therefore, they are explained separately. The dissimilarity appeared, as evidenced in Section 4. In Figure 4, these are identified as dots of different colors.

For convenience, the station is written as station identification (ID) rather than each station location. Station IDs are in accordance with (Augustine et al. 2000). Station group distinction and station ID are specified in Table 1.

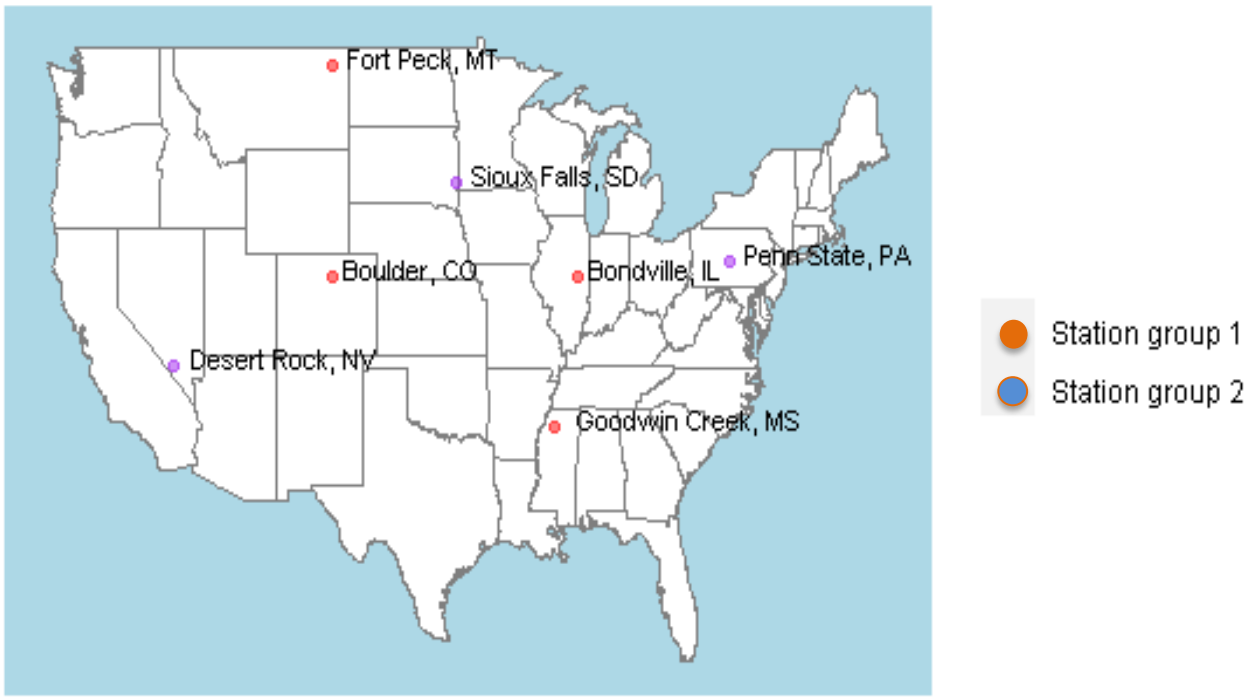

Figure 6. Seven stations in the SURFRAD network.

Table 1. Station information

ID	name	group	start date in raw data	coverage period in this paper
BON	Bondville, IL	1	Jan 1995	Jan 1995 - Dec 2023
FPK	Fort Peck, MT	1	Jan 1995	Jan 1995 - Dec 2023
GWN	Goodwin Creek, MS	1	Jan 1995	Jan 1995 - Dec 2023
TBL	Table Mountain, Boulder, CO	1	June 1995	Jan 1996 - Dec 2023

ID	name	group	start date in raw data	coverage period in this paper
DRA	Desert Rock, NV	2	Mar 1998	Jan 1999 - Dec 2023
PSU	Penn. State Univ., PA	2	June 1998	Jan 1999 - Dec 2023
SXF	Sioux Falls, SD	2	June 2003	Jan 2004 - Dec 2023

For the stations TBL, DRA, PSU, and SXF in which data is observed from the middle of the first year of observations, we use data from the second year for analysis. The data in the first year at FPK is used, on the other hand, because data began in late January and the loss of information is relatively small. For each station, the start date of the raw material and the period considered are written in the 4th and the 5th columns of Table 1.

The differences in the analysis results are also examined and interpreted by dividing data into daytime and all-day. The reason for using the daytime data, as well as, all-day data is due to speculation that the average annual solar irradiance, calculated using the all-day data, reflects the values below zero of night-time, and is, therefore, underestimated. If the daytime is defined as the part of a day between sunrise and sunset, it is necessary to define daytime for each station and for each month. A downwelling diffuse solar measurement is used in the raw data to determine when these times are.

2.4. Global Horizontal Irradiance

The question whether insolation (also referred as **solar radiance** at ground level) has been increasing over time on Earth's ground can be evidence of the B-field weakening. Therefore, the data will reveal if the average of Earth's horizontal irradiance, the total irradiance from the sun on a horizontal surface on the Earth, has an increasing trend over time. This subsection further describes how to calculate Earth's horizontal irradiance at a certain time from raw data and make it an annual variable called 'annual mean Earth's horizontal irradiance'. This is the variable used for analysis. The abbreviation G is used for convenience.

The best measure of the Earth's horizontal irradiance is the algebraic combination of direct-normal solar ($direct\_n$) and downwelling diffuse solar ($diffuse$), as mentioned in (Augustine et al., 2005; NOAA, 2005) using the following equation:

$$Global\ horizontal\ irradiance = direct\_n \cdot cos(SZA) + diffuse$$

Where the SZA is the solar zenith angle, the global horizontal irradiance can be calculated by two variables: $diffuse$ and $direct$. If the two variables are not of good quality due to measurement equipment or weather problems, etc., the variable 'downwelling global solar' in files is employed instead.

The preprocessing phase of computing the 'annual-mean-global-horizontal-irradiance' from scratch is explained as follows: First, only observations with 'minute' variables of 0,30 were extracted from the raw data to reduce the size of the data. The daily mean-global-horizontal-irradiances with the values calculated by the above-mentioned method are then obtained. Some can be seen in the form of outliers if the missing or unreliable values are concentrated in the daytime or night-time (or for all-day) in a day. Outliers are the values that are located far away from the trend. Such observations are all considered to be missing values and imputed with a Kalman-smoothing using the 'imputeTS' package (Moritz & Bartz-Beielstein, 2017) in R programming language. Kalman-smoothing was chosen as this (along with na_seadec) yields reasonable results. The 365-day (or 366-day for leap years) averages of daily mean

global horizontal irradiance for each year 'Annual (A) mean-global-horizontal-irradiance (G)' were called. This is the variable used for analysis. The abbreviations A and G is used for convenience.

3. Adopted Analytical Method and Metrics

3.1. Simple Linear Regression

To establish the increasing trend of solar insolation on Earth's surface over the years, a simple linear regression model was applied. This method finds a relationship (a straight line) between two continuous variables. It is used to predict dependent variable values by a function of a single independent variable. In this case, 'year' was set on the independent variable and '(A) mean-global-horizontal-irradiance (G)' on the dependent variable with the following relationship:

$$\hat{G} = \beta_0 + \beta_1 \cdot year$$

where $\hat{G}$ is the estimated true mean of G for the population for a given year. An intercept 'β_0' is the average value of G when year is 0. A slope 'β_1' is the expected change in G associated with a 1-unit increase in the value of year. β_0 and β_1 are determined by least square estimation (LSE). The fitted straight line will be shown graphically along with '(A) mean-global-horizontal-irradiance (G)' calculated as described in Section 2.

For each station, each linear regression is fitted for the daytime and all-day data. For this, station index s is defined as $s \in \{BON, FPK, GWN, TBL, DRA, PSU, SXF\}$ and time index t as $t \in \{d, a\}$ to indicate whether the data is daytime (d) or all-day (a). These station indexes and time indexes are written in the parenthesis above the abbreviations of our interest. The year index, i, is put on the bottom of them. $n^{(s)}$ indicates the number of years observed in station s. For example, $G_6^{(BON,d)}$ represents the '(A) mean-global-horizontal-irradiance (G)' of the 6-th year (the year 2000 for this station) for the daytime data at station Bondville, IL.

3.2. Evaluation Metrics

Various metrics were used to determine how much solar activity on the Earth's surface has increased (or decreased) over the period. To begin with, the following metrics are based on the value $\hat{G}$, obtained by simple linear regression. An estimate of annual increasing amounts of G at station s at time t ($AAG^{(s,t)}$) can be defined by the following equation:

$$AAG^{(s,t)}(wm^{-2}/year) = \frac{\hat{G}_{n^{(s)}}^{(s,t)} - \hat{G}_1^{(s,t)}}{n^{(s)}}.$$

This represents how much the amount has increased on average each year. Note that this is equivalent to the slope estimate of simple linear regression analysis.

Instead of the difference between the two values, the increase in proportion is compared. An estimate of increasing rate of G relative to the first year observed at station s at time t($RG^{(s,t)}$) can be defined as follow:

$$RG^{(s,t)}(\%) = \frac{\hat{G}_{n^{(s)}}^{(s,t)} - \hat{G}_1^{(s,t)}}{\hat{G}_1^{(s,t)}} \times 100.$$

However, because all stations have different observed years, scaled values are required about the observation year period. If the irradiance had increased the same rate every year and the amount increased were imposed at the end of each year, the following equation for station s at time t is established:

$$\hat{G}_1^{(s,t)}(1+r)^{(n^{(s)}-1)} = \hat{G}_{n^{(s)}}^{(s,t)}$$

where r is the rate of the yearly increase. Therefore, an estimate of compounding annual increasing rate of G at station s at time $t(CARG^{(s,t)})$ can be defined as:

$$CARG^{(s,t)}(\%) = \left\{ \left(\frac{\hat{G}_{n^{(s)}}^{(s,t)}}{\hat{G}_1^{(s,t)}} \right)^{\frac{1}{n^{(s)}-1}} - 1 \right\} \times 100.$$

The results of the statistical significance test regarding AAGs is also analyzed. For each analysis, p-value has to do with 'the annual increasing amount (AAG) and is effective statistically. This is obtained by conducting Student's t-test of the slope of the regression coefficient in a simple linear regression model. The smaller the p-value, the stronger the availability that you should reject the assumption that the slope is 0. That means the estimated coefficient is significant. 'Significance' in tables, shown in section 4, marked as '*' if p-value is less than 0.05, '.' if the value between 0.05 and 0.1, and ' ' if the p-value is greater than 0.1. Usually, if the p-value is less than 0.05, the estimate is considered very significant.

4. Results, Interpretations and Summary of Data

The analysis results by Station group and time (by all-day and daytime) are closely studied in this section.

4.1. Results at Station Group 1

4.1.1. All-day Data

Figure 7 shows graphs of (G) and prediction values of linear regression ($\hat{G}$) through the years for all-day data of Station group 1. Each grid represents the stations in Station group 1. In each graph, the fluctuating blue line stands for G, and the red line is $\hat{G}$. In addition, the bond around the straight line is 95% confidence interval for the mean response.

Solar Cycle 25, which started in 2023, is expected to peak with 115 sunspots in July 2025. Visible light images from NASA's Solar Dynamics Observatory show the Sun at solar minimum in December 2019 (indicated by brackets) and the last solar maximum in April 2014. The previous solar cycle 24 had a maximum in 2014 and a minimum 2009. Hence the data collected, even though cycle 24 shows an increase in (G) is during three solar cycles.

Note: Solar activity, as reported in Figure 7, indicates a decreasing trend (yellow dash line), while our data concludes an increasing trend of solar irradiance at Earth's ground level.

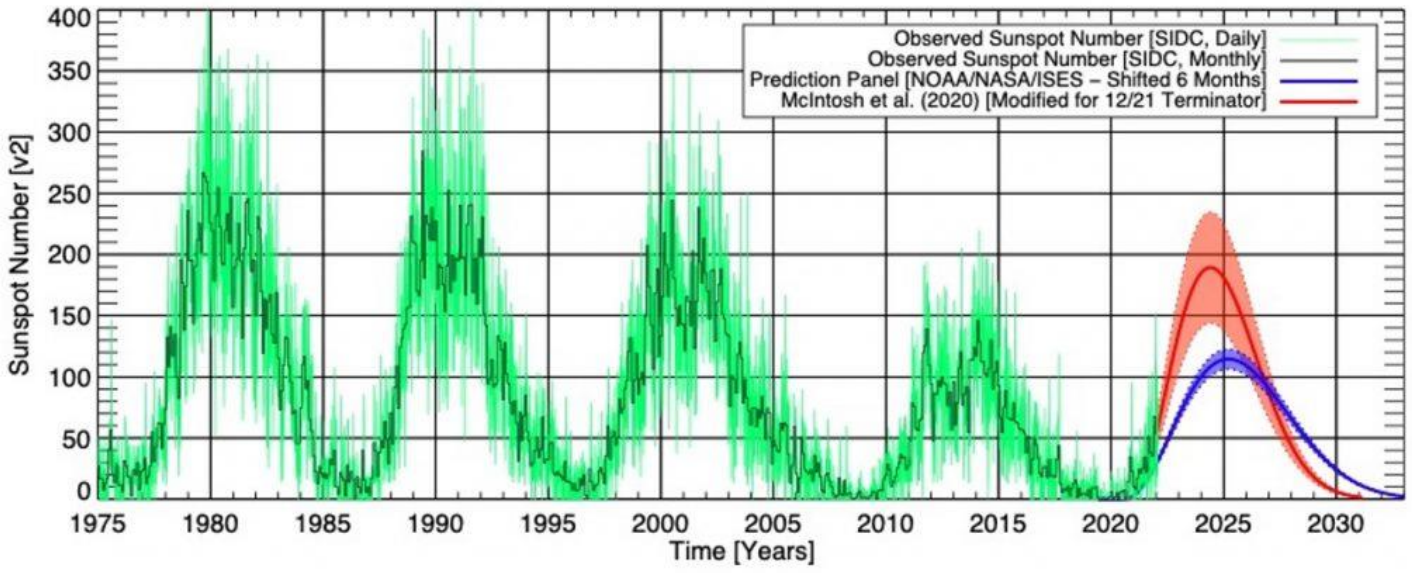

Figure 7. Solar Cycles 21 to 25. Scott McIntosh of National Center for Atmospheric Research, published in Solar Physics

Figure 8 is a split image showing the difference between an active Sun during solar maximum (on the left, captured in April 2014) and a quiet Sun during solar minimum (on the right, captured in December 2019). December 2019 marks the beginning of Solar Cycle 25, and the Sun's activity will once again ramp up until solar maximum, predicted for 2025.

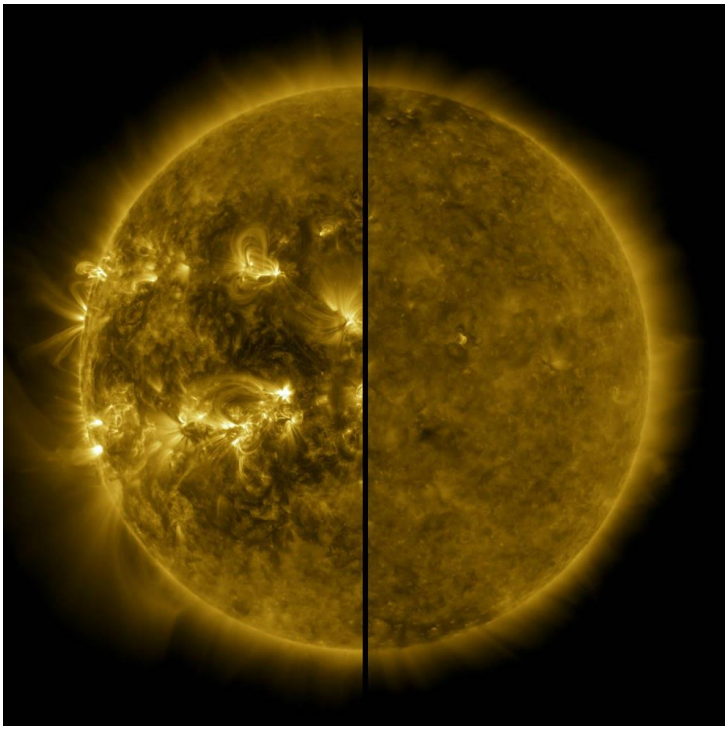

Figure 8. Split image of an active Sun during solar maximum and a quiet Sun during solar minimum. Credits: NASA/SDO

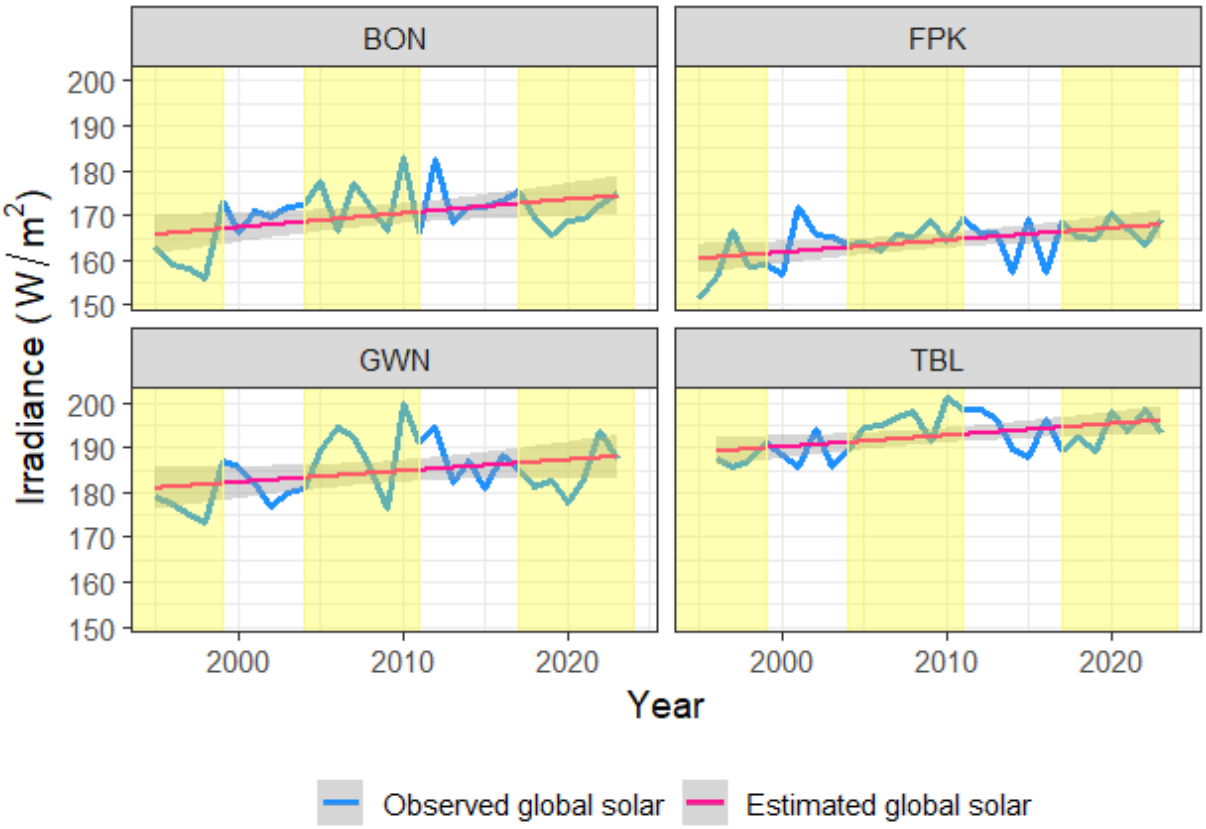

Figure 9. Observed and estimated 'annual-mean-global-solar-irradiance' for daytime data at Station group 1. (Yellow highlights solar minimum)

Figure 9 shows that for all grids, G is fluctuating, but $\hat{G}$ is upward sloping. Figure 9 trend shows that, in the long run, the all-day average of Global horizontal irradiance in Station group 1 is increasing every year. This can be associated with the numbers in Table 2. The table shows the metrics, and the significance test results for AAG. As observed in Table 2, AAG, RG and $CARG$ are all positive values, indicating that solar irradiance on the Earth's surface is on the rise.

Table 2 Evaluation metrics and statistical hypothesis test results for all-day data at Station group 1

Station ID	AAG	RG	CARG	p-value	significance	period (year)
BON	0.3092	5.2227	0.1820	0.0245	*	29.00
FPK	0.2689	4.6945	0.1640	0.0107	*	29.00
GWN	0.2506	3.8773	0.1360	0.0886	.	29.00
TBL	0.2577	3.6793	0.1339	0.0145	*	28.00
Average	0.2716	4.3685	0.1540	0.0346	*	28.75

The average for all stations increased by $0.2716 w/m^2$ each year and increased by 0.1540% per year. It increased by **4.3685% over 28.75 years**. We mention that there is a difference in measurement characteristics between AAG and RG (or $CARG$). In the ratio calculation, the denominator contains the predicted value of the first year, ($\hat{G}_1$), which is relatively large.

By station, the risen amount and rates are the largest in the BON. (The order of increase of AAG, RG and $CARG$ is consistent for the stations.) It increased by $0.3092 w/m^2$ per year and increased by 0.1820% per year. It increased **5.2227% over 28 years** from 1995 to 2023. FPK and TBL follow BON. Meanwhile, GWN has the smallest amount and rates of increase. In addition, the test results of risen amounts were strongly significant for all the other stations. The p-value is 0.0886, and there is less sufficient evidence to reject the null hypothesis with β_1 of 0 at GWN than at other stations. To infer why, you can check that the variation in GWN is large in Figure 7, so the difference between the actual observation G and the straight line is greater than those of the other stations. This means that the standard error is large at GWN. This factor has an adverse effect on proving the significance of β_1.

4.1.2. Daytime Data

Figure 10 is a set of graphs that display G and $\hat{G}$ for the daytime data of four stations in Station group 1. See Section 4.1.1 above for the explanation of two lines with different colors and the bond.

Figure 10. Observed and estimated 'annual-mean-global-solar-irradiance' for daytime data at Station group 1. (Yellow highlights solar minimum)

For the daytime data, $\hat{G}$is also right-upward and increases throughout the years for all grids. That is, the daytime average-global-horizontal-irradiance has increasing trends. Figure 10, compared to Figure 7, the scales of the y-axis and the exact numbers are different, but line at each station does not seem to differ much from the line in pattern for all-day data. The metrics and statistical hypothesis test values are also shown in Table 3.

Table 3 Evaluation metrics and statistical hypothesis test results for daytime data at Station group 1

Station ID	AAG	RG	CARG	p-value	significance	period (year)
BON	0.5412	4.7276	0.1651	0.0401	*	29.00
FPK	0.3997	3.6814	0.1292	0.0399	*	29.00
GWN	0.4829	3.8160	0.1338	0.1020		29.00
TBL	0.5091	3.7676	0.1371	0.0123	*	28.00
Average	0.4832	3.9982	0.1413	0.0486	*	28.75

The average for all stations in Table 3 increased by $0.4832w/m^2$ per year, and by 0.1413% per year. It increased **3.9982% over 28.75 years**. When they are compared with the values in Table 2, AAG has been increased by less than twice, but RG and $CARG$ values are not much different than AAG. This is also due to the characteristics of metrics. The reason that the value of AAG in all-day data is much smaller than in the daytime data is because the value of 0 in the nighttime zone offsets the positive values in the day-time zone when the average G is calculated.

By station, there is the largest increase of the amount and rates in the BON, as with all-day data. It increased by $0.5412w/m^2$ per year, and by 0.1651% per year. It increased by **4.7276% over 28 years** from 1995 to 2023. The TBL follows BON, followed by FPK and GWN. The risen amount is the smallest in FPK, while the rates are the smallest in GWN. p-value and significance columns prove strong significance in TBL and weak significant results in BON and FPK. On the contrary, in GWN, there is no evidence to reject the null hypothesis, β_1 of zero, with p-value 0.1020. The large difference between the actual observation G and the straight line and the small estimate of β_1 would have poorly affected the statistical significance of β_1.

4.2. Results at Station Group 2

4.2.1. All-day Data

Figure 11 is a set of graphs of G and $\hat{G}$ for all-day data for Station group 2. In all stations, the trend line of $\hat{G}$ has a merely right-upward tendency, even if it just seems flat. Table 4 lists the relevant metrics and significance test results. The averages on the bottom line indicate that AAG, RG, and $CARG$ are positive. It increased slightly by $0.0406w/m^2$ per year, by 0.0209% per year and by **0.4474% for a total of 23.33 years**.

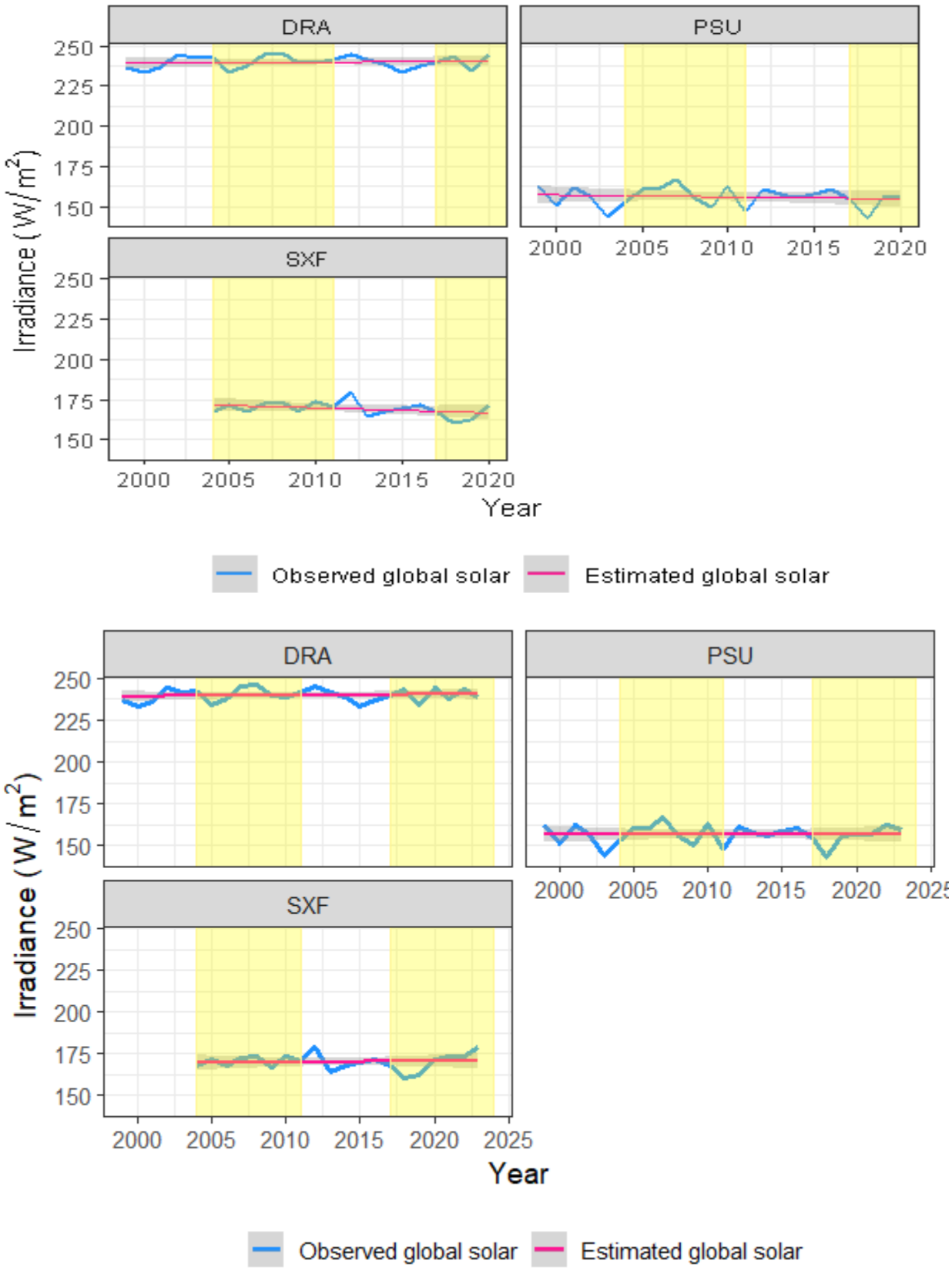

Figure 11. Observed and estimated 'annual-mean-global-solar-irradiance' for all-day data at Station group 2. (Yellow highlights solar minimum).

Table 4 Evaluation metrics and statistical hypothesis test results for all-day data at Station group 2

Station ID	AAG	RG	CARG	p-value	significance	period (year)
DRA	0.0558	0.5595	0.0233	0.6118		25.00
PSU	0.0101	0.1556	0.0065	0.9526		25.00
SXF	0.0560	0.6271	0.0329	0.7775		20.00
Average	0.0406	0.4474	0.0209	0.7806		23.33

By station, in the DRA, both amount and rates have positive values. It increased by $0.0558 w/m^2$, that is, increased by 0.0233% per year, and by $\mathbf{0.5595\%}$ **over a total of 25 years**. Solar horizontal irradiance increased by $0.0560 w/m^2$ and 0.0329% per year at SXF. It increased by $\mathbf{0.6271\%}$ **over 20 years**. PSU follows SXF and DRA. The columns of the p-value and significance marks in Table 4, however, the p-values are greater than 0.1 for all stations in Station group 2. It cannot be concluded that β_1 is different from zero by these numbers. This certainly means that the solar irradiance on the surface neither increased nor decreased statistically at these stations. Then why do these results come out? A valid hypothesis can be that the number of samples (the number of years observed) is relatively small at each station in Station group 2. The small number of samples can affect the statistical hypothesis test results.

Figures 9 and 11 provide another possible cause. Observation values of G appear smaller in the late 1990's than in the 2000's. The growth rates from the late 1990's to the early 2000's seem steep. This factor seems to have made the slope larger in Station group 1. Station group 2's observations, on the contrary, do not have data from the late 1990's. Hence, the lines' slopes are likely estimated to be small in this group. Therefore, the numbers in Table 4 should be used with a degree of confidence. In addition to that, analyses should be examined in a longer-term using more data from a statistical point of view.

4.2.2. Daytime Data

Figure 12 represents G and $\hat{G}$ for the daytime data of Station group 2. The trend of $\hat{G}$ (red line) for each station has a horizontal-like straight line at DRA and SXF, and a slightly right-descending straight lines at PSU. These tend to be like those in Figure 10. The scale of the y-axis is much larger than that of Figure 10 because Figure 12 uses daytime data. Table 5 lists metrics and signification test results for these. The average of all stations in this group increased by $0.0634 w/m^2$, 0.0150% per year. It also increased $\mathbf{0.3164\%}$ **over a total of 23.33 years**.

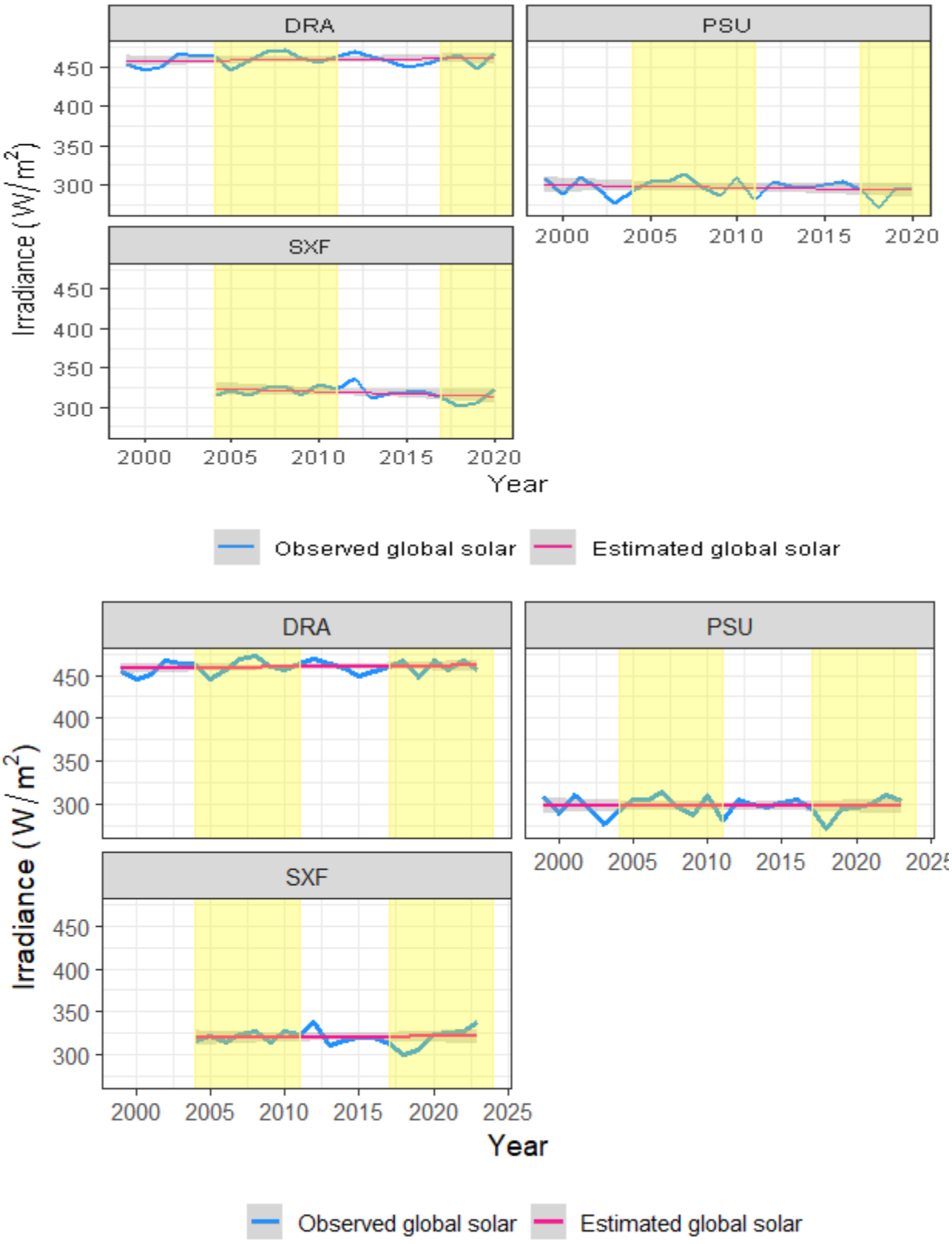

Figure 12. Observed and estimated 'annual-mean-global-solar-irradiance' for daytime data at Station group 2. (Yellow highlights solar minimum)

Table 5 Evaluation metrics and statistical hypothesis test results for daytime data at Station group 2

Station ID	AAG	RG	CARG	p-value	significance	period (year)
DRA	0.1417	0.7426	0.0308	0.5250		25.00
PSU	-0.0394	-0.3174	-0.0132	0.8985		25.00
SXF	0.0881	0.5239	0.0275	0.8158		20.00
Average	0.0634	0.3164	0.0150	0.7464		23.33

By station, the DRA has positive values for the increment and rate of increase parameters. It increased by 0.1417% , by $0.0308 w/m^2$ annually, and by 0.7426% throughout 25 years. SXF has had solar irradiance increase by 0.0275% , by $0.0881 w/m^2$ per year, and by 0.5239% over a total of 20 years. On the other hand, PSU has negative values. Solar horizontal irradiance $0.0394 w/m^2$ and 0.0132% per year at PSU. It decreased by 0.3174% over 25 years. Note that the annual increase or decrease amounts are almost double or more different from all-day data in the same group. As mentioned in 4.1.2, this is a feature of the nature of the data. However, it is interesting that they differ more than the all-day and daytime data differences (see Table 2 and 3) in Station group 1. Unlike the amounts, the ratios of all-day and daytime data are not much different.

Nevertheless, there is no reliability of AAG figures in the Daytime data at these stations. This can be seen in the p-values and significance marks in Table 5. P-values are greater than 0.1 for all stations. The same reasons, mentioned in Section 4.2.1, seem to lead to the results that these AAG figures are not significant.

4.3 Summary of Data

Figure 13 is the yearly average solar activity for daytime for Station group 1 shown in Section 4.1.2. A straight red line is extended to the dotted line of up to 2028. In addition, the area between the red line and the expected solar irradiance of the first year at each station has been shaded.

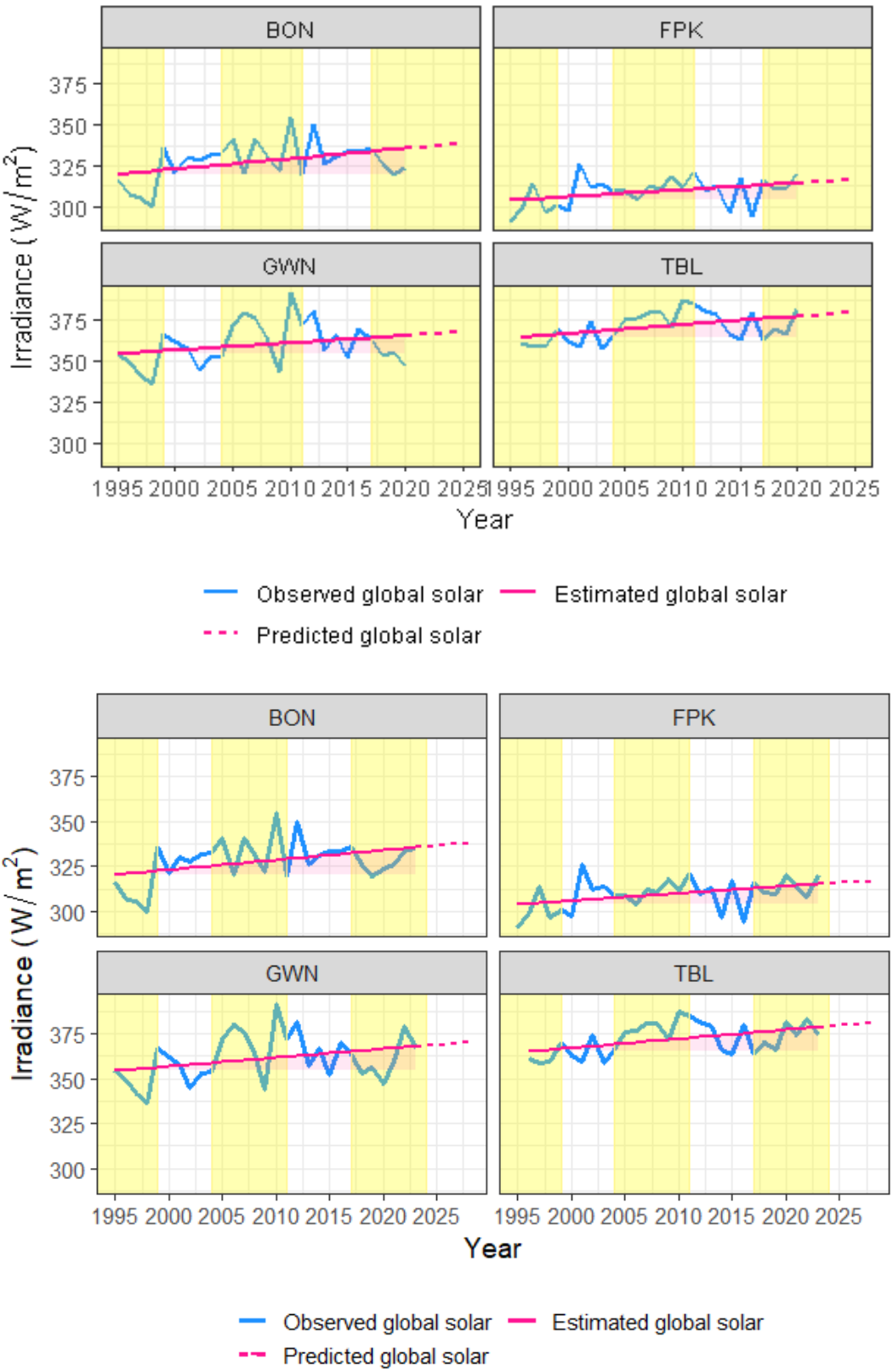

Figure 13. Predicted 'annual-mean-global-solar- irradiance' with observed and estimated values for daytime data at Station group 1. (Yellow highlights solar minimum).

In the 28 years from 1995 to 2023, the expected global solar irradiance at **BON increased by $\mathbf{15.1540 W/m^2}$**. Assuming an annual increase of the same rate, the **global solar activity expectation will increase by $\mathbf{17.8601 W/m^2}$ from 1995 to 2028**. Table 6 is a table of the expected increasing amounts over 33 years, for stations BON, FPK, GWN and TBL.

Table 6. Estimated increasing amount over 30 years at some time in daytime at Station group 1

Station ID	Estimated increasing W/m^2 amount over 33 years
BON	17.8601
FPK	13.1907
GWN	15.9350
TBL	16.8016
Average	15.9468

How large is the expected change in the intensity of sunlight at $\mathbf{17.8601 W/m^2}$ over 33 years in BON? The expected insolation increased will be compared with the amount of electricity produced worldwide in 2008. If this amount of solar energy in Illinois could be converted into electricity, it would be about **30% of the total power output of all power plants in the world**.

To be specific, total world electricity production was $8.9TW$ in 2022 (Wikipedia, 2024). Total area in Illinois is $149{,}998km^2$ and we assume that all points receive the same. It results **in $\mathbf{17.8601 W/m^2}$** $\times$ $10^6 m^2/km^2 \times 149{,}998 km^2 \times 1TW/10^{12}W = 2.6790TW$.

According to a recent research paper (Augustine and Hodge, 2021), solar insolation on the Earth's surface has decreased since 2012. To refute this claim, Figure 14 is a time series of anomalies obtained from the data we preprocessed and based on their method. Ours includes data for 2020 to 2023, and there are some minor differences in preprocessing data. Figure 14 confirms that the insolation increased again since 2019. Furthermore, if linear trend is separately derived for data in 2012 – 2023 (Please see Figure 15 for your reference), as in (Augustine and Hodge, 2021), the slope is positive and a t-test result of the trend of increasing is significant with p-value less than 0.1.

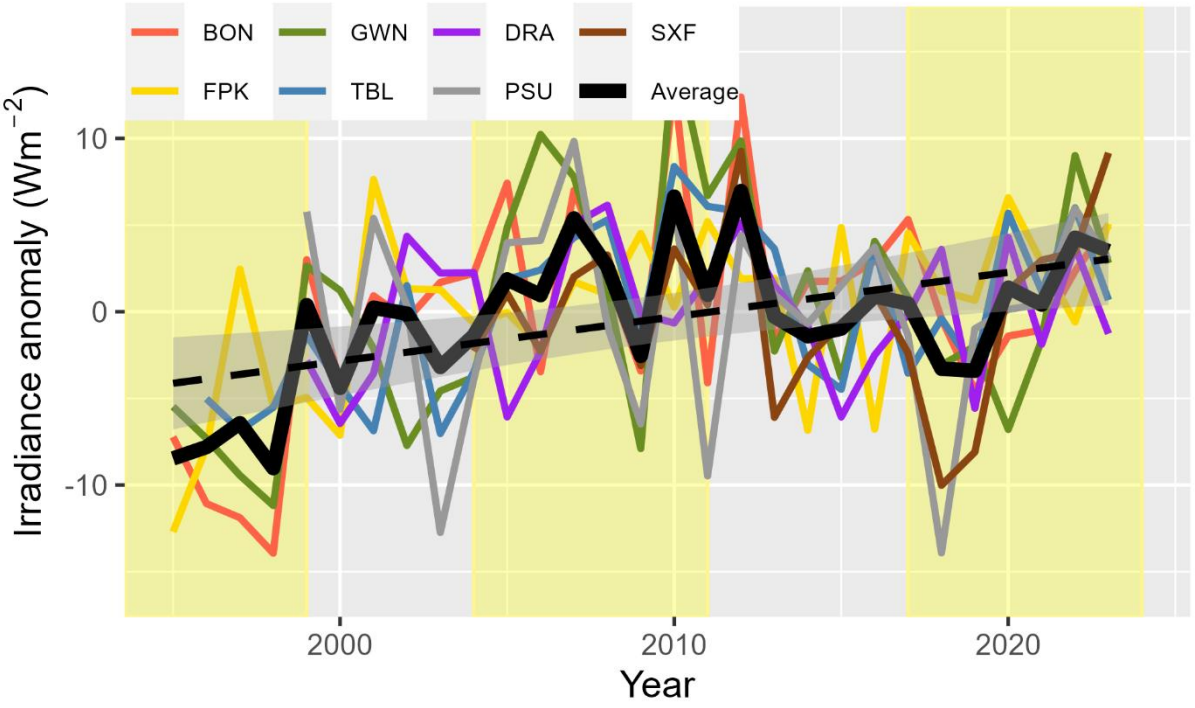

Figure 14. 'annual-mean-global -solar-irradiance' anomalies for the SURFRAD Network. (Yellow highlights solar minimum).

The horizontal zero line in Figure 14 is the overall average of G for all stations for all periods. A thick black line represents the average for each year for all stations. Each colored line is anomaly for each station. A black dashed line is a least-square estimate of the network average value. The bond around the dashed line is a 95% confidence interval of the linear fit. Compare it with Figure 2 in (Augustine and Hodge, 2021). (Augustine and Hodge, 2021) separate the above into two parts along year 2012. The downward trend after 2012 is attributed to some phenomena. Our paper hypothesizes that the phenomena is the solar minimum and therefore, the average value for G should continue and not be segregated.

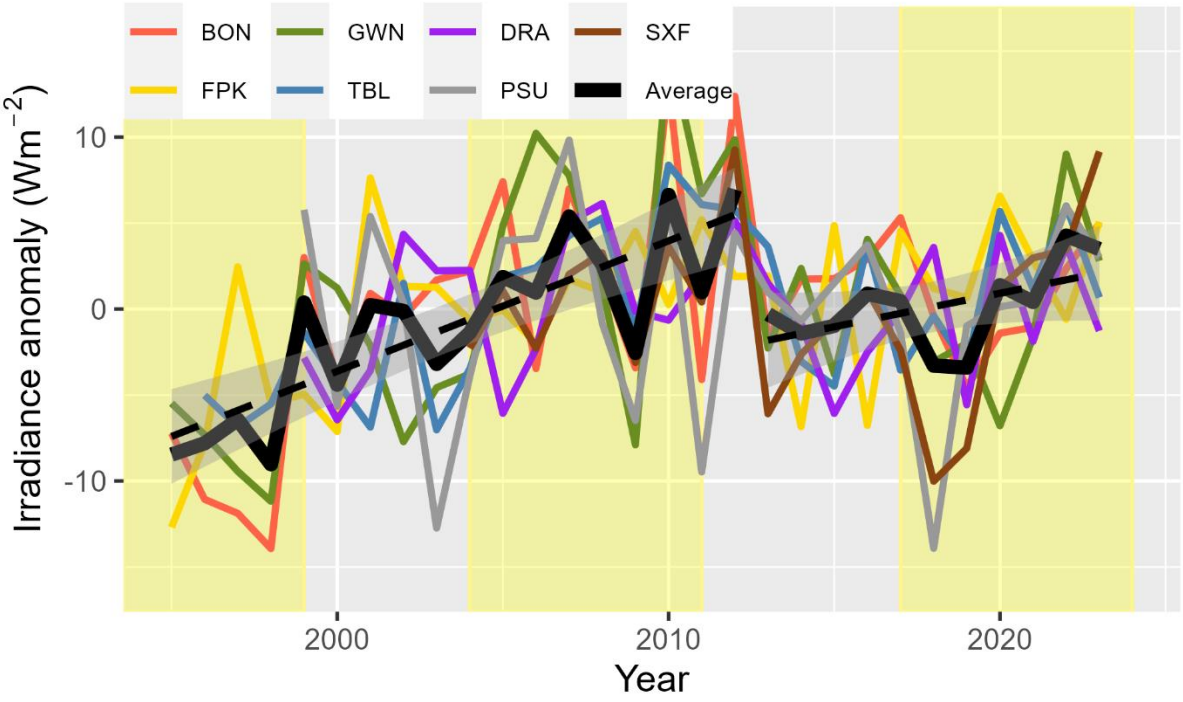

Figure 15. 'annual-mean-global -solar-irradiance' anomalies for the SURFRAD Network. The linear trend is separatedly derived for data from 2012-2023 by others.

5. Comments and Conclusion

Section 4 was analyzed to determine whether the solar irradiance on Earth's surface increases in stations covering various climates in the United States by looking at graphs and numbers. There were increases in all stations except the PSU for daytime data. The increases were especially dramatic in the late 1990s. Statistical hypothesis tests demonstrated the validity of an increase of solar irradiance in BON, FPK, GWN and TBL stations for all-day data and in BON, FPK and TBL stations for daytime data. **Assuming an increase of $17.8601 W/m^2$ for 33 years in Illinois, this is about 30% of the total global production**. It can be concluded that the change in solar irradiance is huge, and the increase could be attributed to the weakening of Earth's B-field.

This paper conducts a basic analysis, assuming a simple straight-line relationship between year and solar horizontal irradiance, which means irradiance increases at the same rate over time.

The research raises further questions for research:

1. The magnitude of the Earth's additional insolation needs to be further defined and its consequences analyzed in relation to global warming trends in conjunction and separate from anthropogenic forcing.

2. What are the atmospheric layers consequences of Earth's magnetic field weakening?

3. What are the consequences of Earth's magnetic field weakening to earth climate?

References

Augustine, J. A., DeLuisi, J. J., & Long, C. N. SURFRAD–A national surface radiation budget network for atmospheric research. *Bulletin of the American Meteorological Society*, (2000) *81*(10), 2341–2358.

Augustine, J. A., Hodges, G. B., Cornwall, C. R., Michalsky, J. J., & Medina, C. I. An update on SURFRAD—The GCOS surface radiation budget network for the continental United States. *Journal of Atmospheric and Oceanic Technology*, (2005). *22*(10), 1460–1472.

Augustine, J. A., Hodges, G. B., Variability of Surface Radiation Budget Components Over the US From 1996 to 2019—Has Brightening Ceased? *Journal of Geophysical Research: Atmospheres*, *126*(7), (2021). e2020JD033590.

Brooks, Michael. "What's wrong with the north pole?" *New Scientist* 242.3236 (2019): 34-37.

Brown, Maxwell, et al. "Earth's magnetic field is probably not reversing." *Proceedings of the National Academy of Sciences* 115.20 (2018): 5111-5116.

Budyko, Mikhail I. "The effect of solar radiation variations on the climate of the Earth." *tellus* 21.5 (1969): 611-619.

Fedorov, V. M., and P. B. Grebennikov. "Calculation of long-term averages of surface air temperature based on insolation data." *Izvestiya, Atmospheric and Oceanic Physics* 53.8 (2017): 757-768.

Fernández-Solís, J. L. "Relations and Implications of Aperiodic Earth Core/Geomagnetic Field Reversals with Earth Glaciations." (2018). Dr. Solis https://oaktrust.library.tamu.edu/handle/1969.1/169361

Harrington, R. This incredible fact should get you psyched about solar power - US Department of Energy (2015) https://www.businessinsider.com/this-is-the-potential-of-solar-power-2015-9

Livermore, Philip W., Christopher C. Finlay, and Matthew Bayliff. "Recent north magnetic pole acceleration towards Siberia caused by flux lobe elongation." *Nature Geoscience* 13.5 (2020): 387-391.

Moritz, S., & Bartz-Beielstein, T. imputeTS: time series missing value imputation in R. *R J.*, (2017). *9*(1), 207.

National Research Council. "Understanding the Sun and Solar System Plasmas: Future Directions in Solar and Space Physics." 2005 Washington, D.C.: The National Academies Press. https://doi.org/20.17226/11188.

NOAA Earth System Research Laboratories. ESRL Global Monitoring Laboratory - Global Radiation and Aerosols. (2005, October 1). Retrieved February 9, 2021, from https://www.esrl.noaa.gov/gmd/grad/surfrad/

Široký, Jan, and Richard Linhart. "Solar storm detecting by integrated magnetometer based on anisotropic magnetoresistivity." *2017 25th Telecommunication Forum (TELFOR)*. IEEE, 2017.

Smulsky, Joseph J. "Insolation Periods of Climate Change as a Means of Solving Long-Term Climatic Puzzles." *Modern Environmental Science and Engineering* 6.2 (2020): 190-201.

Vervelidou, Foteini, et al. "On the accuracy of palaeopole estimations from magnetic field measurements." *Geophysical Journal International* 211.3 (2017): 1669-1678.

Wikipedia. Electricity generation. (2024, January 10). Retrieved January 14, 2024., from https://en.wikipedia.org/wiki/Electricity_generation.

Yang, D. Solar Data: An R package for easy access of publicly available solar datasets. *Solar Energy*, (2018). *171*, A3–A12.

Further Reading

Bärenzung, Julien, et al. "Modeling and Predicting the Short-Term Evolution of the Geomagnetic Field." *Journal of Geophysical Research: Solid Earth* 123.6 (2018): 4539-4560.

Cai, Shuhui, et al. "Archaeointensity results spanning the past 6 kiloyears from eastern China and implications for extreme behaviors of the geomagnetic field." *Proceedings of the National Academy of Sciences* 114.1 (2017): 39-44.

Chalk, Thomas B., et al. "Causes of ice age intensification across the Mid-Pleistocene Transition." *Proceedings of the National Academy of Sciences* 114.50 (2017): 13114-13119.

Hasenfratz, Adam P., et al. "The residence time of Southern Ocean surface waters and the 100,000-year ice age cycle." *Science* 363.6431 (2019): 1080-1084.

Kapper, Lisa, et al. "Reconstructing the geomagnetic field in West Africa: first absolute intensity results from Burkina Faso." *Scientific reports* 7.1 (2017): 1-12.

Kozyreva, Olga V., et al. "Ground geomagnetic field and GIC response to March 17, 2015, storm." *Earth, Planets and Space* 70.1 (2018): 1-13.

Laskar, J., F. Joutel, and F. Boudin. "Orbital, precessional, and insolation quantities for the Earth from-20 Myr to+ 10 Myr." *Astronomy and Astrophysics* 270 (1993): 522-533.

Palencia-Ortas, A., et al. "New archaeomagnetic directions from Portugal and evolution of the geomagnetic field in Iberia from Late Bronze Age to Roman Times." *Physics of the Earth and Planetary Interiors* 270 (2017): 183-194.

Panovska, Sanja, M. Korte, and C. G. Constable. "One hundred thousand years of geomagnetic field evolution." *Reviews of Geophysics* 57.4 (2019): 1289-1337.

Panovska, Sanja, C. G. Constable, and Monika Korte. "Extending global continuous geomagnetic field reconstructions on timescales beyond human civilization." *Geochemistry*, *Geophysics*, *Geosystems* 19.12 (2018): 4757-4772.

Paluš, M., and D. Novotná. "Northern Hemisphere patterns of phase coherence between solar/geomagnetic activity and NCEP/NCAR and ERA40 near-surface air temperature in period 7–8 years oscillatory modes." *Nonlinear Processes in Geophysics* 18.2 (2011): 251-260.

Reddmann, T., Sinnhuber, M., Wissing, J. M., Yakovchuk, O., & Usoskin, I. (2023). The impact of an extreme solar event on the middle atmosphere: a case study. *Atmospheric Chemistry and Physics*, *23*(12), 6989-7000.

Stern, Robert J., and Nathan R. Miller. "Neoproterozoic Glaciation—Snowball Earth Hypothesis." *Age (Ma)* 632.1.0 (2019): 632-3.

Tema, Evdokia, Emilio Herrero-Bervera, and Ph Lanos. "Geomagnetic field secular variation in Pacific Ocean: A Bayesian reference curve based on Holocene Hawaiian lava flows." *Earth and Planetary Science Letters* 478 (2017): 58-65.

Katoh, Y., Rosendahl, P. S., Ogawa, Y., Hiraki, Y., & Tadokoro, H. (2023). Effect of the mirror force on the collision rate due to energetic electron precipitation: Monte Carlo simulations. *Earth, Planets and Space*, *75*(1), 117.